https://doi.org/10.5194/essd-2022-306
Preprint. Discussion started: 14 September 2022

Open Access Earth System Science Data Discussions

Water masses distribution in the Canadian Arctic Archipelago: Implementation of the Optimal MultiParameter analysis (OMP)

Alessandra D'Angelo[1], Cynthia Garcia-Eidell[2], Christopher Knowlton[3], Andrea Gingras[1], Holly Morin[3], Dwight Coleman[3], Jessica Kaelblein[3], Humair Raziuddin[2], Nikolas VanKeersbilck[4], Tristan J. Rivera[5], Krystian Kopka[6], Yoana Boleaga[6], Korenna Estes[7], Andrea Nodal[8], Ericka Schulze[5], Theressa Ewa[2], Mirella Shaban[5], Samira Umar[2], Rosanyely Santana[9], Jacob Strock[1], Erich Gruebel[3], Michael Digilio[6], Rick Ludkin[10], Donglai Gong[11], Zak Kerrigan[1], Mia Otokiak[12], Frances Crable[2], Nicole Trenholm[13], Triston Millstone[14], Kevin Montenegro[9], Melvin Kim[14], Gibson Porter[12], Tomer Ketter[15], Max Berkelhammer[2], Andrew L. King[16], Miguel Angel Gonzalez-Meler[2], and Brice Loose[1]

[1]University of Rhode Island, Graduate School of Oceanography, Narragansett, RI 02882, USA
[2]University of Illinois at Chicago, Chicago, IL 60607, USA
[3]Inner Space Center, University of Rhode Island Graduate School of Oceanography, Narragansett, RI 02882, USA
[4]The University of Iceland at Reykjavik, 102 Reykjavík, Iceland
[5]Virginia Commonwealth University, Richmond, VA 23284, USA
[6]City University of New York, City College, NY 10031, USA
[7]California State University Fresno, Fresno, CA 93740, USA
[8]Oregon State University, Corvallis, OR 97331, USA
[9]Florida International University, Miami, FL 33199, USA
[10]Haldimand Bird Observatory, Ontario, Canada
[11]Virginia Institute of Marine Science, Gloucester Point, VA 23062, USA
[12]Nunavut Impact Review Board, Nunavut, Canada
[13]University of Maryland, College Park, MD 20742, USA
[14]California State University Channel Islands, Camarillo, CA 93012, USA
[15]University of New Hampshire, Durham, NH 03824, USA
[16]Norwegian Institute for Water Research, 0579 Oslo, Norway

Correspondence to: Alessandra D'Angelo (a_dangelo@uri.edu)

https://doi.org/10.5194/essd-2022-306
Preprint. Discussion started: 14 September 2022

Abstract

The Canadian Arctic Archipelago (CAA) acts as a watershed discharge in the Arctic Ocean, as it is characterized by advection from the Pacific and Atlantic waters, ice melt, local river discharge and net precipitation. Its waters are characterized by the mixing of Pacific and Atlantic water origin, and the meltwater supply originating from the Devon Ice Cap Glaciers and marine-terminating rivers. The Special Report on the Ocean and Cryosphere in a Changing Climate published by the IPCC in 2021, showed how the runoff into the Arctic Ocean increased for Eurasian and North American rivers by 3.3 ± 1.6% and 2.0 ± 1.8% respectively (1976–2017), hence, monitoring the freshwater supply within the CAA is crucial in a warming scenario. This paper aims to describe the water mass structures within the CAA, by analyzing physical and chemical tracers collected in 2019 during the Northwest Passage expedition held in July and August onboard the Swedish icebreaker Oden. The uniqueness of this study is the wide dataset composed of physical and chemical parameters (https://doi.org/10.18739/A2W66995R). Here, we implemented the Optimal Multiparameter analysis for the detection of the source water fractions, such as, Atlantic Water (AW), Pacific Water (PW), Meteoric Water (MW), and Sea Ice Meltwater (SIM). For this analysis, we used a nutrient ratio tracer defined Arctic Nitrate-Phosphate tracer, together with the absolute salinity and $\delta^{18}O$ from the water samples. Our analysis confirmed the intrusion of the PW from the west in the upper layers and of AW from the east in the deeper layers. We also discriminated the meltwaters between glacial and sea ice origin and showed their spatial distribution in the study area. This study provides unique set of data from this under observed region and can serve as baseline for further analysis and continued data collection.

https://doi.org/10.5194/essd-2022-306
Preprint. Discussion started: 14 September 2022

1. Introduction

The Beaufort Gyre in the western Arctic Ocean is the largest oceanic freshwater reservoir in the northern hemisphere (Carmack et al., 2016). The Canadian Arctic Archipelago (CAA) and the downstream Davis Strait, rather than Fram Strait, are the main pathways through which Beaufort Gyre freshwater exits the Arctic Ocean into the North Atlantic Ocean (Zhang et al., 2021). Recent studies (Zhang et al., 2021) showed increased CAA freshwater transport dominated by water from the Beaufort Gyre region as compared to other regions of the Arctic. The Arctic and CAA are also global hotspots of change due to the warming climate, which could affect freshwater supply and transport. The potential for increases in ice-free open waters and the proximity to areas of deep-water formation has implications for global carbon cycling and has cascading effect for the highly productive marine ecosystem. Therefore, detecting the contribution of the waters characterizing the CAA is crucial in a changing Arctic. This region is home to Inuit communities that depend on the ocean for sustenance, and there is a growing list of anthropogenic impacts including shipping, tourism, fishing, gas/oil production, etc. To improve our understanding of the state of this vulnerable environment, we developed a synoptic study, in order to assess the water mass contributions in/out of the CAA.

1.1 Study area

The study area was located within Parry Channel, between 71 – 77 ºN, and 100 – 79 ºW, within the central CAA (Fig. 1). This area puts in connection Baffin Bay with Beaufort Sea, eastern and western sides, respectively.

https://doi.org/10.5194/essd-2022-306
Preprint. Discussion started: 14 September 2022

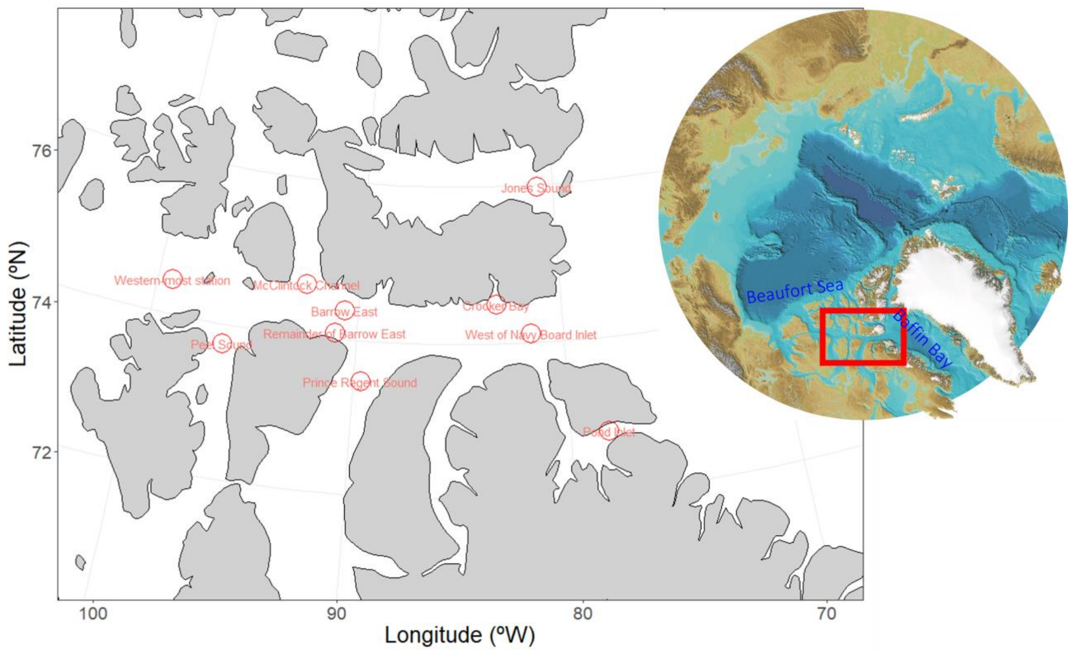

Figure 1: On the left, study area with sampling locations during the Northwest Passage cruise, July – August 2019. On the right, the international bathymetric chart of the Arctic Ocean (IBCAO), with a highlight on the Parry Channel (red rectangle).

The Northwest Passage Project (NPP) took place in July and August 2019 across the CAA onboard the Swedish Icebreaker Oden (expedition NWP2019). Sampling consisted of transects, often longitudinal in orientation, in order to catch the inward and outward water flow for assessment of meltwater transport.

1.2 Meltwater input

The CAA is indeed characterized by advection from the relatively fresh upper layers of the Arctic Ocean, ice melt, local river discharge and net precipitation (e.g., Ingram & Larouche, 1987). The limiting sill of the Parry Channel is located further east in Barrow Strait where the depth is ~125 m. Continuing eastward water depths again increase gradually to ~ 500m in Lancaster Sound, then increase rapidly to over 2000 m in the center of Baffin Bay (Shimada et al., 2005; Mclaughlin et al., 2007). The general direction of the surface flow is from the Pacific to Arctic to Atlantic Oceans, due to geostrophy and the higher sea-level of the Pacific (Shimada et al., 2005). This sea level difference occurs because Pacific waters are fresher and,

https://doi.org/10.5194/essd-2022-306
Preprint. Discussion started: 14 September 2022

assuming a level of no-motion among the three ocean basins, the Arctic is thought to be 0.15 m higher than the Atlantic (Stigebrandt, 1984). The shallow sill (~125 m) at Barrow Strait restricts the flow eastward across Lancaster Sound (LS), constraining the penetration of the deeper layer of AW (Shimada et al., 2005; Mclaughlin et al., 2007). Here, the riverine runoff supplied by Cunningham River, Garnier River and Mecham River has a big effect on the hydrodynamics and biogeochemistry of Parry Channel (Brown et al., 2020). The Special Report on the Ocean and Cryosphere in a Changing Climate published by the IPCC in 2021, showed how the runoff into the Arctic Ocean increased for Eurasian and North American rivers by 3.3 ± 1.6% and 2.0 ± 1.8% respectively (1976–2017). Another forcing affecting hydrodynamics in LS is the tidal energy. It enters the CAA mainly from the Atlantic Ocean and is mainly semi-diurnal. As a result, waters transiting Parry Channel are significantly modified by tidally-driven mixing and, in the vicinity of Barrow Strait, tidal currents are especially strong, reaching 50–150 cm s^{-1} (Melling et al., 1989).

1.3 Water column characteristics

The water column structure is characterized by AW in the deep layers, with Pacific-origin waters overlaid, and seasonal mixed water at the top (Mclaughlin et al., 2007). In the summer, the seasonal mixed layer contains fresh water from watershed runoff and sea-ice melt and is characterized by low salinities ($24<S<31$), warm temperatures, low nutrient concentrations, and high dissolved oxygen saturations. This water is the upper-most layer and its depth changes accordingly to the meltwater supply (~ 50 m thick in Parry Channel). Below this layer is the Pacific-origin summer water. This water is characterized by relatively warm temperatures, higher salinities ($31<S<32$), and nitrate deficit relative to phosphate. Recent studies (Zhuang et al., 2021)showed extreme nitrate deficit extended to greater depths and further north during the past two decades, which coincided with the expansion of Pacific water in the western Arctic Ocean. Atlantic-origin water, within bottom layers, shows higher temperatures, salinities (~ 34) and maximum nutrient concentrations (Shimada et al., 2005). The western part of the CAA is characterized by a more consistent sea-ice coverage (Agnew and Howell, 2003). The information released by the Canadian Ice Service show that the ranges of sea ice thickness of first year ice in the CAA varies from maximum values of 2.5 m in the northern and 2.0 m in the southern sections. Multi-year ice can reach a thickness of 3–5 m (Canadian Ice Service, 2002). Between freeze-up in January and break-up in late July the ice is generally immobilized by attachment to the land (landfast ice) and due to strong winds, it is also characterized by the occurrence of polynyas (Dunbar, 1969).

2. Data and methods

https://doi.org/10.5194/essd-2022-306
Preprint. Discussion started: 14 September 2022

During the expedition, 53 CTD (conductivity, temperature, and depth) casts were deployed, collecting a total of six transects and three stations for the hydrographic investigation. The CTD rosette carried 24 Niskin bottles with GPS coordinates directly fed to the CTD deck unit. A SeaBird SBE 911+ CTD with dissolved oxygen and WETLabs Ecopuck sensors were mounted on the SeaBird 32 Water Carousel CTD rosette. The CTD sensor was owned and calibrated by the Swedish Polar Research Secretariat (SPRS). The parameters measured through the sensors were, temperature, salinity, dissolved oxygen, fluorescence, and turbidity (Table S1, S2). Moreover, we also sampled water for oxygen isotopes and macronutrients (nitrate+nitrite, phosphate, silicate) (Table S2). The data presented in this study includes samples collected from: Jones Sound (4 stations), Pond Inlet (1 station), West Navy Board Inlet (6 stations), Croker Bay (2 stations), Peel Sound (6 stations), Barrow East (7 stations), Prince Regent Sound (8 stations), McClintock Channel (6 stations), Western-most station (1 station) (Fig. 1). CTD casts and rosette bottle data will be hosted at Arcticdata.io and the CCHDO public databases.

2.1 Data

The physical data were coupled with tracers for investigating water mass identification. For salinity and temperature, we used absolute salinity (SA) and conservative temperature (CT), respectively, calculated through the Gibbs Sea Water tools in “gsw package” in R version 4.1.2 in RStudio Version 1.2.5033 (Table S1). The other tracers used in this manuscript are the oxygen isotope 18O ($\delta^{18}O$), and the Arctic Nitrate-Phosphate (ANP) tracer (Newton et al., 2013; Whitmore et al., 2020) (Table S2). The sea ice concentration data was provided by the University of Illinois at Chicago (UIC), using daily SB2 sea ice concentration data with spatial resolution of 6.25 km (Comiso et al., 2017). For the raster plot of the sea ice concentrations, we used the data provided by the University of Bremen data archive, with 10m resolution (seaice.uni-bremen.de, Spreen et al., 2008). The methodological steps of the next sections are used to develop a dataset providing information about the water mass identification and contribution.

2.1.1 Nutrients

Silicate, phosphate, nitrate, and nitrite concentrations were determined using a Quik Chem Series 8500 Lachat analyzer (Serial Number 061100000379 – Hach, Loveland, Colorado, USA). Heater Configuration 500 W Max, reagents and standards prepared using Quik Chem Protocols: Nitrate + Nitrite 31-107-04-1 A, Silicate 31-114-27-1 A, Phosphate 31-115-01-1 H. The analysis was carried out at the Marine Science Research Facility, GSO – URI. To quality check the nutrients data, we did the comparison between dataset

https://doi.org/10.5194/essd-2022-306
Preprint. Discussion started: 14 September 2022

from literature (e.g., Bhatia et al., 2021), data storage, and our data. When all the measured nutrients (Phosphate, Nitrate+Nitrite, Silicate) showed agreement with the reference data, a flag = 1 was assigned to the values, meaning reliable data. We also tried to identify the outliers through other procedures, but these did not show high efficiency for our dataset. For example, we calculated the N:P:Si ratios for near Redfieldian consistency, however, this method could not be appropriate for our data, since denitrification plays a big part in shaping the nutrient ratios in Pacific waters, and significant freshwater inputs enhance to not utilize nutrients in a Redfieldian manner. Nutrient ratios were combined to form quasi-conservative water-mass tracers, to identify the contribution of the water masses within the mixing layers. To quantify the distribution and amount of the seawater in the CAA, we used nutrients in a four-component linear endmember mixing model. Previously, nutrients, combined in their Redfield ratios, have been used to separate Pacific- and Atlantic-derived waters (Ekwurzel et al., 2001; Whitmore et al., 2020). We calculated the Arctic Nitrate-Phosphate tracer (ANP), following Newton et al. (2013). Here, ANP was determined through the Euclidean geometry, by calculating the distance between the sample and the Pacific and Atlantic trendlines, equations 3 and 4 (Jones et al., 1998; Whitmore et al., 2020 – Fig.2).

$$NO_3{}^{-}{}_{AW} = (17.499 * [PO_4]^{3-}) - 3.072 \tag{1}$$

$$NO_3{}^{-}{}_{PW} = (12.368 * [PO_4]^{3-}) - 10.549 \tag{2}$$

$$ANP_{AW} = \frac{abs(5.6-17.499*0.2+3.072)}{sqrt\,(1^2)+(7.499^2)} \tag{3}$$

$$ANP_{PW} = \frac{abs(5.6-12.368*0.2+10.549)}{sqrt\,(1^2)+(12.368^2)} \tag{4}$$

https://doi.org/10.5194/essd-2022-306
Preprint. Discussion started: 14 September 2022

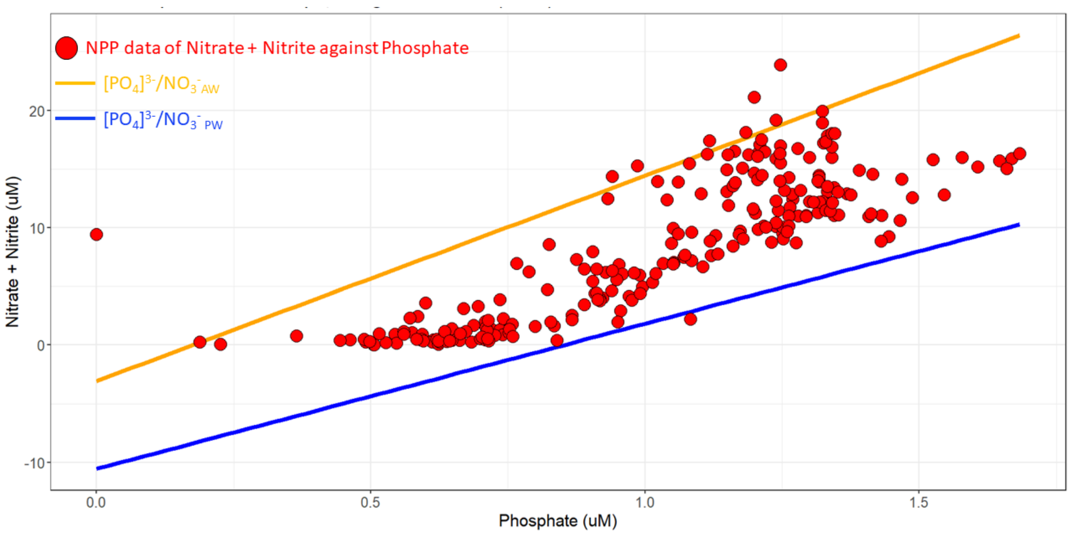

Figure 2: Nitrate-Phosphate relationships, using Jones 1998 model, including data from the cruise (red dots). The orange line represents $[PO_4]^{3-}$ / $NO_3^-{}_{AW}$ for Atlantic waters, while the blue line is $[PO_4]^{3-}$ / $NO_3^-{}_{PW}$ for Pacific waters.

ANP is essentially a version of the N* tracer, adapted to the specific N/P ratios of the Arctic water column and scaled to the dynamic range of the pelagic Arctic Ocean (Newton et al., 2013). It is impacted by processes other than photosynthesis and respiration, which cause departures from Redfield ratios. The principal non-Redfield factors are bacterial nitrification and denitrification, which take place mainly in the anoxic regions of the continental shelf benthos (Newton et al., 2013). This is the reason why the ANP fits well in our dataset.

2.1.2 Oxygen isotopes data

To help identify water mass endmembers for freshwater budgeting, we collected matching $\delta^{18}O$-Salinity data from discrete samples from the surface (bucket sampling) and from profiles (CTD casts). Here, we will show the data collected from the CTD casts. The $\delta^{18}O$-Salinity dataset which contains more than 200 new and paired $\delta^{18}O$-Salinity measurements in the CAA is publicly available through Pangaea: https://doi.pangaea.de/10.1594/PANGAEA.937543.

https://doi.org/10.5194/essd-2022-306
Preprint. Discussion started: 14 September 2022

A total of 125 matching measurements were collected at varying depths from 52 CTD casts. The CTD rosette water sampling was conducted following the CLIVAR/GO-SHIP protocol with a 'water cop' keeping track of the sampling order. Samples for water stable isotopes analyses were collected by filling 30-mL Nalgene bottles to the brim. Bottles were closed tightly, sealed with parafilm, and stored in a labeled sample bag. Sampling depths chosen were based on the profile, location, and whether samples were collected for nutrients. Two samples were collected per depth. The corresponding salinity and temperature measurements per sampling depth were collected from the CTD data. All water samples were transported to the Atmosphere, Climate, and Ecosystems lab at the UIC for processing. The δ^{18}O and dD were measured using a Picarro l2130-I CRDS water isotope analyzer with a wire mesh inserted in the vaporizer inlet to trap salt from the seawater. Fifteen injections were made for each sample and necessary corrections to address 'memory effect' were employed. Measurements were normalized using the dD and δ^{18}O values of internal water standards.

The amount of the oxygen isotopes (N=125 samples) collected during the cruise did not always coincide with the location and quantity of physical and chemical data (N=238 sample), therefore the final amount of available δ^{18}O data was 52. This data was only available at discrete locations (Fig. 3), though these locations spanned the range of water mass space. Therefore, it was possible to extend the OMP analysis to all the ship based CTD data. We sought to use both the oxygen isotopes and the nutrient measurements as water mass tracers, hence we applied an extension of δ^{18}O OMP solutions to CTD data, where the CTD and depth matched, using the same approach proposed by (Beaird et al., 2017).

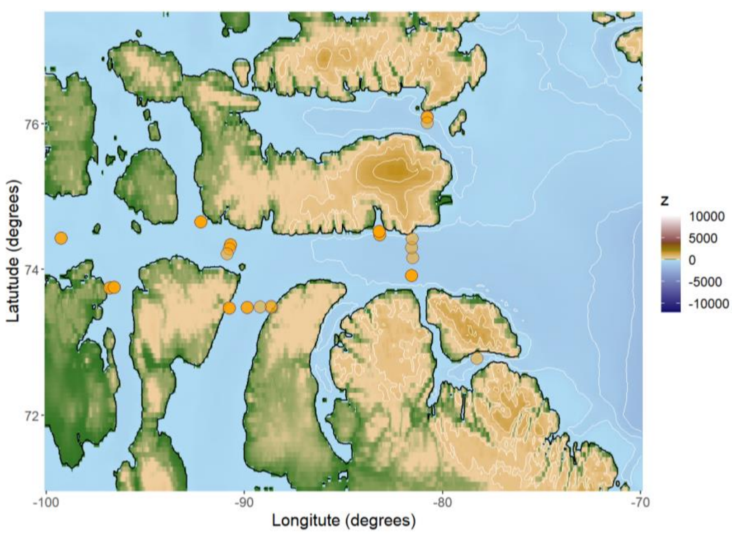

https://doi.org/10.5194/essd-2022-306
Preprint. Discussion started: 14 September 2022

Figure 3: Top view map of the study area, with orange dots displaying the oxygen isotopes data matching the nutrients and CTD data sites.

We used a traditional three-endmember water mass analysis in local regions to fill in the gaps in the $\delta^{18}O$ results CT/SA space (Fig. 4). The extension was made by defining a series of non-overlapping triangular elements in CT/SA space whose vertices are at oxygen isotopes observation points (Beaird et al., 2017).

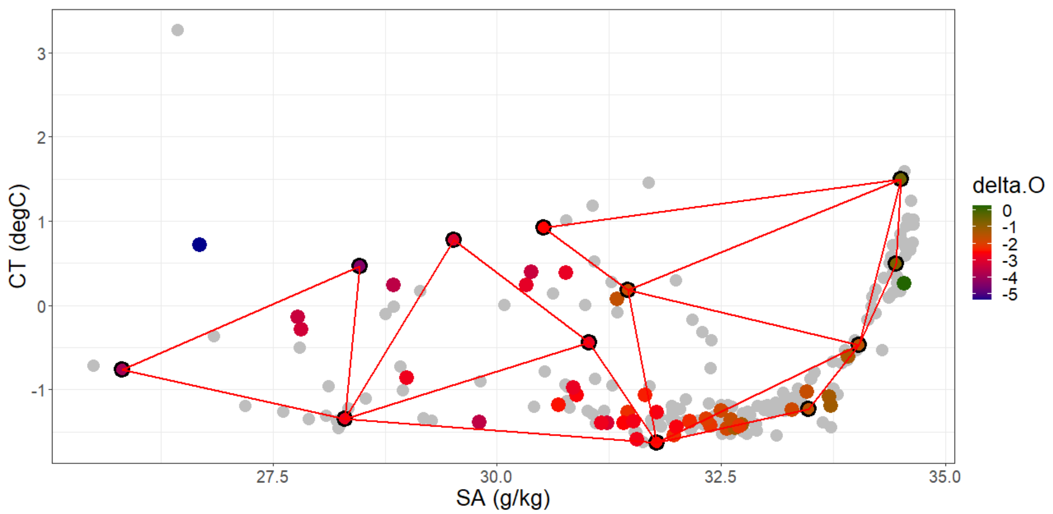

Figure 4: Conservative temperature against absolute salinity plot of ship-based CTD observations (gray dots), $\delta^{18}O$ sample points "delta.O" (magnitude showed by the color scale) and triangular elements (red lines) for the three-endmember method to extend oxygen isotopes OMP solutions to all CTD data.

We assumed that within these regions local mixing sets properties and therefore points inside each bounded region could be written as a combination of the properties at the vertices – as in classical water mass analysis. We first found the relative contribution of each vertex to a given observation point in CT/AS space (a three-endmember mixing model), then we used the fact that we know the water mass content of those vertices (from the $\delta^{18}O$ OMP) to derive the water mass content at the observation location (see Appendix in Beaird et al., 2017). The final dataset was of length 195 over the 125 of the original oxygen isotopes.

https://doi.org/10.5194/essd-2022-306
Preprint. Discussion started: 14 September 2022

2.1.3 Water mass defined by linear mixing model

The water samples were assumed to be a mixture of several idealized end members or 'water types' (Tomczak and Liefrink, 2005), whose physical and chemical characteristics have been well characterized (source water masses, SWM). The Optimal Multiparameter analysis is based on the following assumptions: (a) the mixing processes between SWMs are linear; (b) the observed properties are conservative and (c) the SWMs properties are accurately known. Additionally, the OMP analyses are constrained to satisfy the mass balance equation at any point (Pardo et al., 2012). The contribution of each SWM (f_i) is estimated for each measured point using an ordinary least squares method. The obtained f_i values are in the range 0–1 and refer to the amount of a certain SWM ''i'' that is implicated in the mixing processes (Pardo et al., 2012; Newton et al., 2013). The SWMs in our study were: Atlantic Water (AW), Pacific Water (PW), Meteoric Water (MW) and Sea Ice Meltwater (SIM). We applied SA, $\delta^{18}O$, and an N:P-based tracer (ANP) to calculate the fractions of each sample. The endmembers were chosen according to our dataset and previous literature (Table 2): for salinity we used both extreme values (for AW and PW) and values from literature for MW and SIM (Whitmore et al., 2020; Newton et al., 2013; Ekwurz et al., 2001); for ANP we followed Newton et al., (2013); finally, for $\delta^{18}O$ we used the extreme values for AW and PW, MW= -20 (Whitmore et al., 2020), and SIM= surface values per CTD + 2.6 ‰ (as in Newton et al., 2013).

$$f_{AW}+f_{PW}+f_{MW}+f_{SIM}=1$$

$$f_{AW}(SA)+f_{PW}(SA)+f_{MW}(SA)+f_{SIM}(SA)=SA_{obs}$$

$$f_{AW}\,(ANP)+f_{PW}\,(ANP)+f_{MW}\,(ANP)+f_{SIM}\,(ANP)=ANP_{obs}$$

$$f_{AW}(\delta^{18}O)+f_{PW}(\delta^{18}O)+f_{MW}(\delta^{18}O)+f_{SIM}(\delta^{18}O)=\delta^{18}O_{obs}$$

Table 2: OMP endmembers. AW, PW, MW, SIM are the source water masses (SWMs); SA is the absolute S (g/kg), ANP is the Arctic nitrate-phosphate tracer, MB is the mass balance; $\delta^{18}O$ was measured in ‰. For SIM, the ANP and $\delta^{18}O$ tracers were calculated as averaged surface values per each CTD station; for $\delta^{18}O$ tracer, we also added 2.6 ‰ as in Newton et al., (2013).

	AW	PW	MW	SIM
SA	34.50	32.50	0	4

https://doi.org/10.5194/essd-2022-306
Preprint. Discussion started: 14 September 2022

ANP	0	1	0	Surface values
$\delta^{18}O$	0	-2.50	-20	Surface values + 2.6
MB	1	1	1	1

All the tracers were standardized as follows:

$$\frac{data - mean(data)}{SD(data)}$$

as they were measured in different measurement units (Table S3). The mass balance component of the matrix was set with a higher weight with respect to the other components, in order to adjust the variables. The weight applied was equal to 0.05

$$MBw = \frac{1}{0.05}$$

2.2 Reproducibility of the 3-endmember method for extending the $\delta^{18}O$ data

The extension we made for expanding the $\delta^{18}O$ data to all the ship based CTD data (Beaird et al., 2017) was quality checked through statistics steps for a $\delta^{18}O$ interpolation 'fit quality'. Initially, we calculated the misfit between the original and interpolated data as:

$$\text{Misfit} = ((\delta^{18}O_{int} - \delta^{18}O)/\delta^{18}O) * 100\ (\%)$$

Where $\delta^{18}O_{int}$ are the values obtained by interpolation and $\delta^{18}O$ are the original data. To visualize, in Figure 5 we showed both the data overlapped against the absolute salinity.

https://doi.org/10.5194/essd-2022-306
Preprint. Discussion started: 14 September 2022

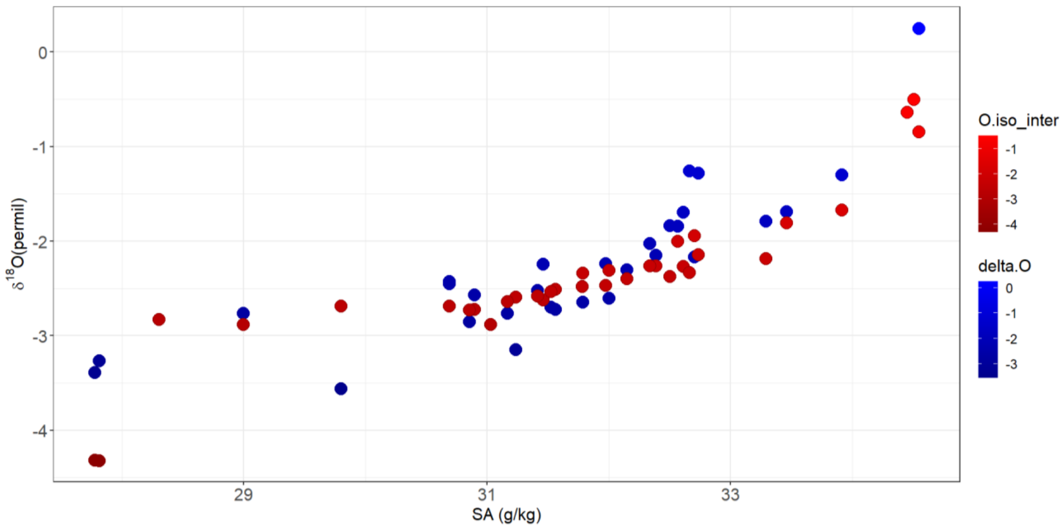

Figure 5: The plot shows the absolute salinity against the original $\delta^{18}O$ and the interpolated ones. The red dots display the data obtained through the interpolation (O.iso_inter), whereas the blue dots show the original $\delta^{18}O$ data (delta.O). Few points are perfectly overlapping, but the misfit was still in a good range of reproducibility (with the mean uncertainty ~8 %).

The second step was calculating the residuals (Fig. S1) on the mass balance and make sure that they did not exceed the SD=5% at every location. Residuals between interpolated and original data were used to identify possible outliers as well as to evaluate the actual scatter in the data set. The success of this three-endmember method was subject to the points in the triangular element that needed to be the product of the interaction of one endmember (Beaird et al., 2017). If the method failed, the system was underdetermined by temperature and salinity observations and errors in interpretation could arise. After observing our results, the misfit between the two datasets, and the residuals, we assessed the $\delta^{18}O$ interpolation 'fit quality'.

2.3 Reproducibility of the OMP analysis

Residuals were minimized to solve the equation; hence we used the set of endmembers showing best fit with the dataset (Fig. 6, Table S3).

https://doi.org/10.5194/essd-2022-306
Preprint. Discussion started: 14 September 2022

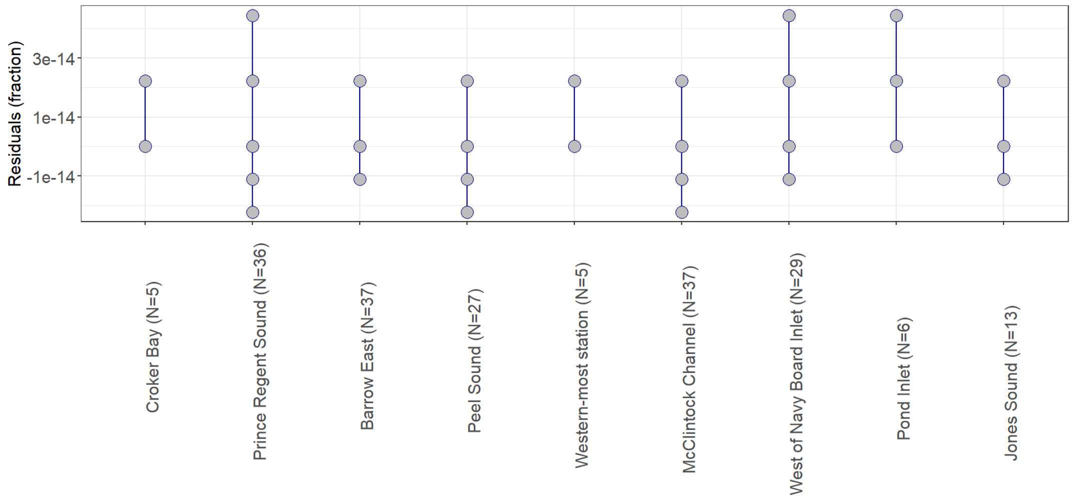

Figure 6: Residuals (fractions) calculated over the OMP analysis by transect. The N represents the number of measurements per transect.

The ordinary least solved through matrix decomposition, by ensuring the number of water properties exceeds the number of source water types in the analysis (Tomczak and Large, 1989). The minimization becomes an over-determined problem and is solved in a straightforward manner since the misfit does not exceed the 5% (Henry-Edwards and Tomczak, 2006).

3. Results

3.1 Identification of the water masses

In Figure 7, the SA (g/kg) and the CT (ºC) profiles of the water masses are shown for every station.

https://doi.org/10.5194/essd-2022-306
Preprint. Discussion started: 14 September 2022

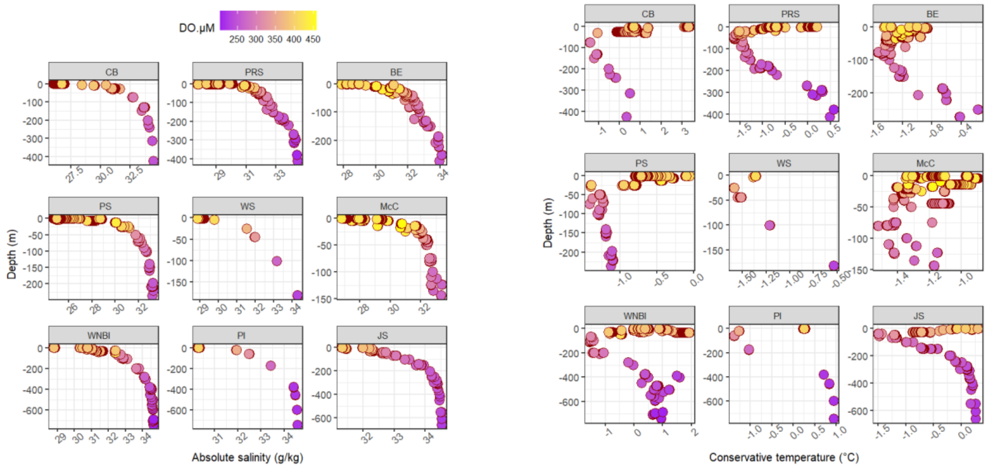

Figure 7: vertical profiles of conservative temperature (ºC) and absolute salinity (g/kg) recorded for every transect. CB (Croker Bay), PRS (Prince Regent Sound), BE (Barrow East), PS (Peel Sound), WS (Western-most Station), McC (McClintock Channel), WNBI (West of Navy Board Inlet), PI (Pond Inlet), JS (Jones Sound). The color scale indicates the dissolved Oxygen (µM).

The overall picture showed negative CT towards the western Channel (up to -1.62 ºC in Prince Regent Sound), with higher temperature recorded eastwards in the AW masses and shallow Polar Mixed Layer (PML, up to 3.38 ºC in Croker Bay station). The occurrence of AW was detected in the deeper layers of the eastern stations, with higher CT and SA (see Fig.7 PRS, WNBI, PI, JS). High CT were also recorded within the shallow Polar Mixed Layer (PML) in CB and WNBI. The major outcome showed that the AW intruded from East at deep layers, likely influenced by the bathymetric barrier, while the entire Channel was PW-origin dominated. The meltwater affected the upper layer (PML) at times up to 40 m depth. This layer was characterized by fresh (SA<30 g/kg) and warm (CT >= 0 ºC) waters.

3.2 Water mass contribution

The OMP analysis showed balanced contribution along the vertical profile of AW and PW (Fig. 8a), with high contribution of freshwater in the upper PML. The contribution of MW and SIM was balanced (Fig. 8b) and it mainly occupied the 10% of the very surface layers. In some sites, the MW reached deep layers, suggesting further investigation about the hydrodynamics of those locations. We recorded a few negative values for MW (6 data points), which suggested an artifact in the extension of δ[18]O data, as it did not show in the OMP including only original data. In Croker Bay, data in the very surface layer (above 30m depth) were omitted due to low 'fit quality' of the δ[18]O interpolation. However, here we recorded high temperatures and the highest freshwater signal for oxygen isotopes. A table with the OMP analysis outcome is shown in the supplementary material, Table S3.

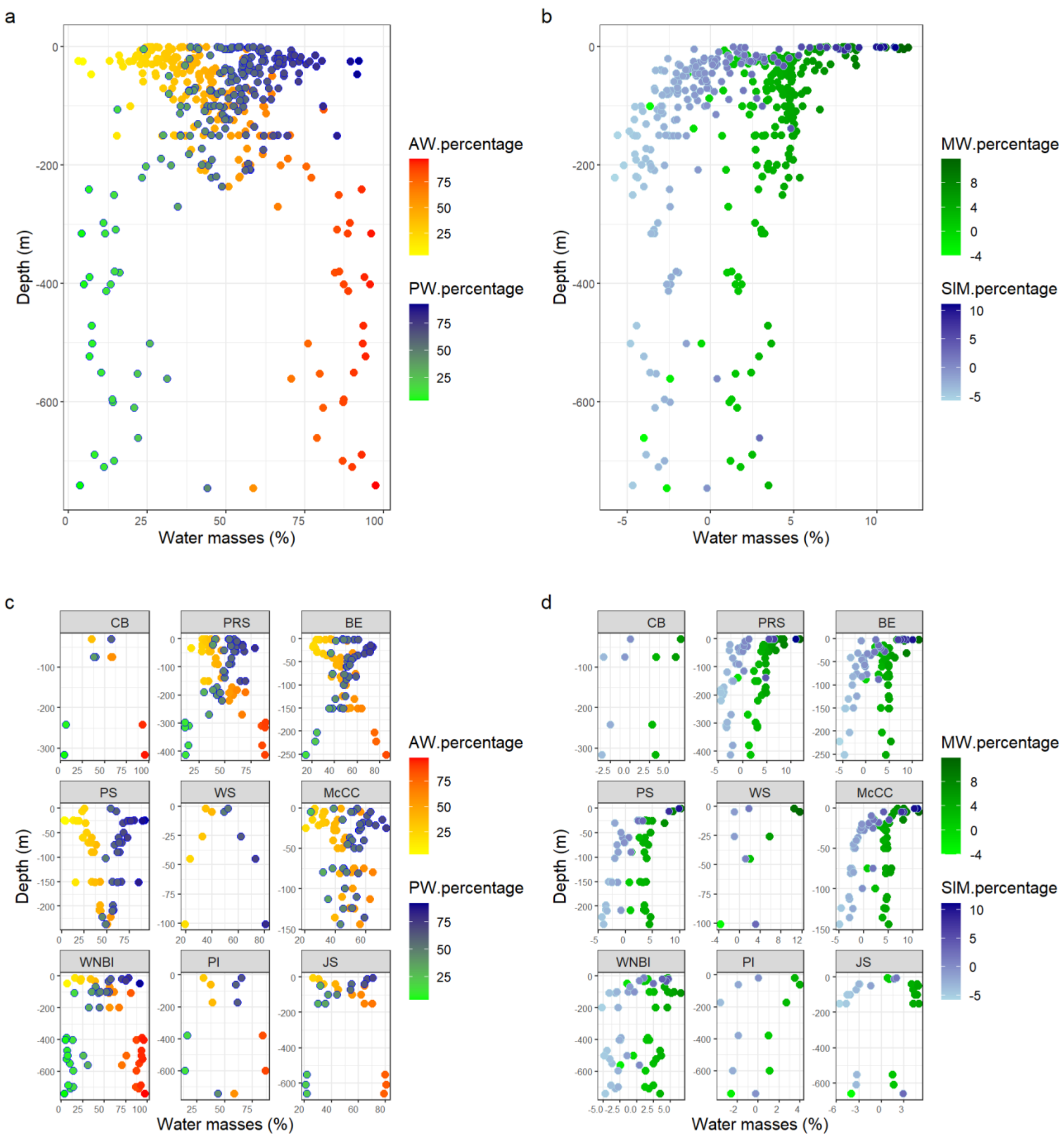

https://doi.org/10.5194/essd-2022-306
Preprint. Discussion started: 14 September 2022

Figure 8: Vertical profiles of water mass contribution (%). a) Vertical profile of all Pacific and Atlantic Waters; b) Vertical profile of all Meteoric and Sea Ice Melt- Waters; c) Vertical profile of Pacific and Atlantic Waters fractions showed by transect; d) Vertical profile of Meteoric and Sea Ice Melt- Waters fractions showed by transect. CB (Croker Bay), PRS (Prince Regent Sound), BE (Barrow East), PS (Peel Sound), WS (Western-most station), McCC (McClintock Channel), WNBI (West of Navy Board Inlet), PI (Pond Inlet), JS (Jones Sound).

The following describes the water mass contributions and characteristics from east to west. Jones Sound showed balanced contribution of Atlantic (max ~ 80%) and Pacific (max ~71%) Waters, with surface layers characterized by higher MW input (av. ~3±2%) and sea ice formation. Pond Inlet was highly influenced by AW intrusion, showing a contribution of MW ~3.5% in the subsurface layers. West of Navy Board Inlet recorded the highest AW fraction (together with Croker Bay) of ~100% within deep layers. The surface layer was characterized by a mix of SIM and MW (>4%), while the subsurface layers were MW dominated (reaching ~7%). In Croker Bay, because of the interpolation method, the dataset is lacking the very surface data (up to 30m), however the $\delta^{18}O$ data recorded the highest freshwater input. In this site, the water column was characterized by high AW contribution (~100%) in deep layers, and high PWs within the upper layer. Barrow East showed a relative balance between Atlantic and Pacific Waters, and between Meteoric Water and Sea Ice Meltwaters. The SIM showed sea ice formation along the water column, while the sea ice coverage was characterized by multi-year ice and thick first-year ice. In Prince Regent Sound the balance between AW and PW was still confirmed. The meltwater contributions also were balanced, however the SIM showed high ice formation signal. Peel Sound was PW dominant (av. ~65±12%), with balanced meltwater input at the surface, and sea ice formation below 25m depth. McClintock Channel was also PW predominant (av. >50%) with the upper layer characterized by mixed meltwaters, overlaying the sea ice formation fraction. Here, the sea ice concentration recorded the highest value (~90%). The western-most station was deeply influenced by the PW intrusion (av. > 60%). Here, the MW dominated the meltwater supply (reaching ~ 12%), while the SIM was very poor. The sea ice concentration was relatively high (~85%) and was characterized by multi-year ice, second stage thin first-year ice and thin first-year ice.

4. Discussion

4.1 Choice of the endmembers

The conservative parameters of salinity and temperature, together with the oxygen isotopes, are widely used from the oceanographic community to assess the contribution of the water masses in the water column. In this study we used the conservative temperature (coupled with absolute salinity) to better represent the heat content of the water masses. Recent studies from the Arctic (e.g., Ekwurzel et al., 2001; Newton et al., 2013; Whitmore et al., 2020) used geochemical tracers to highlight specific freshwater components in a different way. Newton et al. (2013) for example, created POs*, a new salinity-dependent version of the PO* tracer to account for the difference in Redfield ratios between Atlantic and Pacific water masses.

$$f = \frac{1}{1 + \exp\left(10 * (34.5 - SA)\right)}$$

$$POs* = (f * \left(Phosphate + \left(\frac{Oxygen}{175}\right) - 1.95\right) + ((1 - f) * (Phosphate + \left(\frac{Oxygen}{125}\right) - 1.95))$$

Qualitatively, the POs*-based results were congruent with results from the Arctic N/P relationship, however the two methods differed in the surface layers where the N/P ratios are potentially impacted by biological processes. Here, the POs* method is also impacted by gas exchange with the atmosphere (Newton et al., 2013). After combining several nutrients ratios to obtain quasi-conservative (aerobic-conservative) water mass tracers, we assessed that the best fitting tracer for our purpose was the Arctic N-P tracer.

4.2 Outcome and previous knowledge

The contribution of AW and PW corroborated observations from previous literature: high inflow of Atlantic origin waters from 200m downward coming from the Baffin Bay were detected, with Pacific water domination on the western Channel (Fig. 10 a, b, white arrows). The PW origin intruded the upper layer and, together with the meltwater, modified into the summer polar mixed layer (Fig. 10 b, red rectangles). For a better visualization, Fig. 10 did not show the meltwaters fractions (displayed in Fig.11a and b).

https://doi.org/10.5194/essd-2022-306
Preprint. Discussion started: 14 September 2022

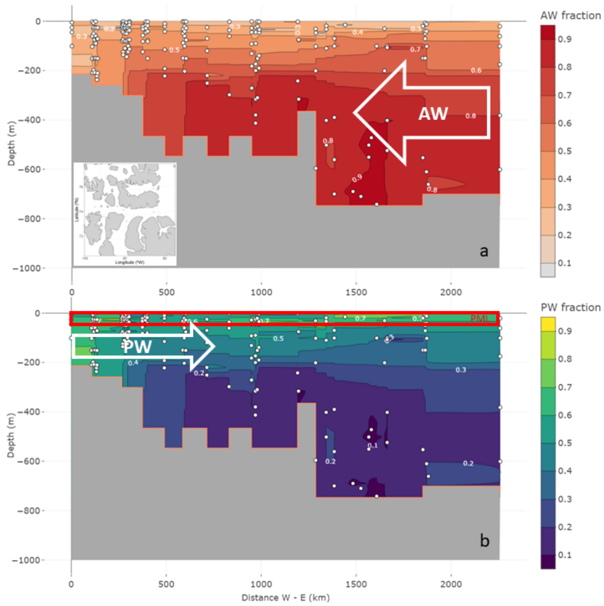

Figure 10: contour plots of water masses contribution across the CAA, a) shows the AW fraction, b) shows the PW fraction. The x axis displays the distances (in km) from the most-western site 0 km (Longitude = 99.2768 ºW) to the most eastern location 2200 km (Longitude = 78.2579 ºW), see the zoom out of the map in plot (a). The white dots show the data points, that are calculated as the averaged values of fractions by transect and depth. This allowed us to graph sections for the contour plots. The longitudinal transects (Peel Sound, McClintock Channel and Prince Regent Sound) are also included in the plots, as their waters are surrounding and influencing the Sound hydrography. The red rectangle represents the Polar Mixed Layer, while the white arrows display the AW and PW intrusions.

The meltwaters showed similar behavior between glacial and sea ice origin, both the supplies mainly originated in the western channel with similar magnitude (see Fig. 11a, b). The highest freshwater input was recorded in Croker Bay (shown by the $\delta^{18}O$ data), however, we could not show this in the figure as the 3-endmember interpolation was removing some data points. Nevertheless, several studies recorded great meltwater runoff at termini of the Devon Ice Cap (Shimada et al., 2005; Grau Galofre et al., 2018; Alkire et al., 2019; Brown et al., 2020), and our data corroborated this outcome at 30 m depth.

https://doi.org/10.5194/essd-2022-306
Preprint. Discussion started: 14 September 2022

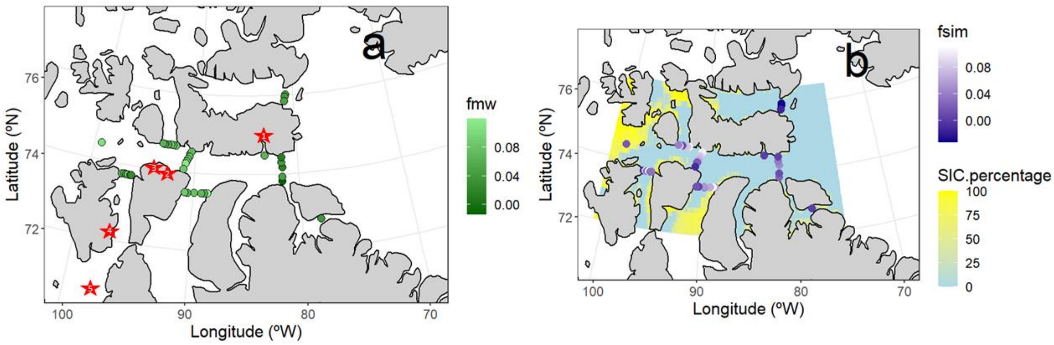

Figure 11: top view map of the area of study, with color scales showing (a) fraction of meteoric waters (fmw), (b) fractions of sea ice meltwaters (fsim), and percentage of sea ice concentration (SIC.percentage). In (a), the red stars indicated the river discharge, star number 5 was in the middle of Peel Sound indicating the numerous rivers flowing from the southern CAA. In (b), the SIC data were downloaded by the University of Bremen data archive at 10m spatial resolution (seaice.uni-bremen.de).

Most of the sites with the highest provision of MW within the CAA were close by the watershed drainage (Brown et al., 2020). In the middle channel, Cunningham River (3), Garnier River (2), and Devon Ice Cap River (1) likely provided a big input of freshwater, while Le Feuvre Inlet (4) and all the southern coastal-draining rivers (5) supplied the western channel (see Fig. 11a). The SIM was mainly spread towards West, with highest contributions occurring in McClintock Channel, Peel Sound, Prince Regent Sound, and Barrow East (Fig. 11 b). Its trend reflected the sea ice coverage, with highest concentrations westward (see Fig. 11b).

5. Data availability

The produced database of this study (D'Angelo et al., 2022) has been archived in Arctic Data Center and can be assessed using the following link: https://doi.org/10.18739/A2W66995R. The database is provided at two different resolutions (OMP matrix and original data). The data of different resolutions can be used as a tool to assess uncertainties associated with the interpolation and OMP calculations.

6. Conclusion

In this study we described the water mass contribution in the Canadian Arctic Archipelago, using the Optimal Multiparameter analysis. We encompassed physical and chemical parameters to provide a unique output on the water mass identification in the CAA. The conservative temperature coupled with absolute salinity was used to better represent the heat content of the water masses and define the source waters. In particular, we implemented and discussed the use of a semi-conservative tracer in the OMP analysis (Arctic N:P – Jones et al., 1998; Ekwurz et al., 2001; Newton et al., 2013) effective to discriminate the Pacific, meteoric and sea ice origin waters. The efficiency of adding this tracer to the 3-endmember matrix resulted in the detection of the surface waters, as this tracer is impacted by processes which take place mainly in the hypoxic/anoxic regions of the continental shelf. We provided detailed descriptions of the analysis developed, including its reproducibility, and we showed the efficiency of applying this method in coastal Arctic seawater. The CAA, characterized by shallow waters (max 800m depth in our study area) and PW dominated, was a relatively simple system contributing to the success of our model. The outcome confirmed a mix of PWs and meltwaters in the surface layers, overlying AW layers. The meltwater provision mainly originated in the western channel (regardless the Devon Ice Cap supply in Croker Bay). We can conclude that our method gave effective outcomes about the PW and AW intrusion from the outer Parry Channel and discriminated the meltwaters origin with a minimum error (residuals ~0). Despite some artifacts in the results, we strongly recommend this method for characterizing the water column structure in Arctic coastal environments.

Author contribution

B.L. and A.D. implemented the study. A.D., B.L., D.G., C.G-E., J.K., H.R., N.V., T.J.R., K.K., Y.B., K.E., A.N., E.S., T.E., M.S., S.U., R.S., J.S., E.G., M.D., R.L., Z.K., M.O., F.C., N.T., T.M., K.M., M.K., G.P., and T.K. were involved in the sampling activities. A.D., B.L., C.G-E., M.B., F.C., A.L.K, and M.A.G-M. performed the analysis and processed the data. C.K., A.G., D.C. organized the logistics and guided the project development. A.D., B.L. and C.G-E. wrote the manuscript with input from all authors. The authors declare that they have no conflict of interest.

Acknowledgements

We would extend our gratitude to the entire crew of the RVIB Oden, and the Swedish Polar Research Secretariat team for the logistic effort. We thank our Arctic guide Sarah Scriver for assistance. We acknowledge the local communities for their collaboration, and the Marine Science Research Facility at GSO - URI, for carrying out the nutrients analysis. The study was supported by the National Science Foundation Awards #1748318 and #1821911, with additional support from the Heising Simons Foundation.

https://doi.org/10.5194/essd-2022-306
Preprint. Discussion started: 14 September 2022

Earth System Science Data Discussions

We gratefully acknowledge the NSF Program Officer for the Northwest Passage Project, Valentine Kass, and the lead PI of the project, Gail Scowcroft (Associate Director, Inner Space Center, University of Rhode Island).

https://doi.org/10.5194/essd-2022-306
Preprint. Discussion started: 14 September 2022

References

Agnew, T. and Howell, S.: The use of operational ice charts for evaluating passive microwave ice concentration data, Atmosphere - Ocean, 41, 317–331, https://doi.org/10.3137/ao.410405, 2003.

Alkire, M. B., Jacobson, A., Macdonald, R. W., and Lehn, G.: Assessing the Contributions of Atmospheric/Meteoric Water and Sea Ice Meltwater and Their Influences on Geochemical Properties in Estuaries of the Canadian Arctic Archipelago, ESTUAR COAST, 42, 1226–1248, https://doi.org/10.1007/s12237-019-00562-w, 2019.

Beaird, N., Straneo, F., and Jenkins, W.: Characteristics of meltwater export from Jakobshavn Isbræ and Ilulissat Icefjord, in: ANN GLACIOL, 107–117, https://doi.org/10.1017/aog.2017.19, 2017.

Bhatia, M. P., Waterman, S., Burgess, D. O., Williams, P. L., Bundy, R. M., Mellett, T., Roberts, M., and Bertrand, E. M.: Glaciers and Nutrients in the Canadian Arctic Archipelago Marine System, GLOBAL BIOGEOCHEM CY, 35, https://doi.org/10.1029/2021GB006976, 2021.

Brown, K. A., Williams, W. J., Carmack, E. C., Fiske, G., François, R., McLennan, D., and Peucker-Ehrenbrink, B.: Geochemistry of Small Canadian Arctic Rivers with Diverse Geological and Hydrological Settings, J Geophys Res Biogeosci, 125, https://doi.org/10.1029/2019JG005414, 2020.

Carmack, E. C., Yamamoto-Kawai, M., Haine, T. W. N., Bacon, S., Bluhm, B. A., Lique, C., Melling, H., Polyakov, I. v., Straneo, F., Timmermans, M. L., and Williams, W. J.: Freshwater and its role in the Arctic Marine System: Sources, disposition, storage, export, and physical and biogeochemical consequences in the Arctic and global oceans, J GEOPHYS RES-BIOGEO, 121, Pages 675-717 https://doi.org/10.1002/2015JG003140, 1 March 2016.

Ekwurzel, B., Schlosser, P., Mortlock, R. A., Fairbanks, R. G., and Swift, J. H.: River runoff, sea ice meltwater, and Pacific water distribution and mean residence times in the Arctic Ocean, J GEOPHYS RES-OCEANS, 106, 9075–9092, https://doi.org/10.1029/1999jc000024, 2001.

Grau Galofre, A., Mark Jellinek, A., Osinski, G. R., Zanetti, M., and Kukko, A.: Subglacial drainage patterns of Devon Island, Canada: Detailed comparison of rivers and subglacial meltwater channels, Cryosphere, 12, 1461–1478, https://doi.org/10.5194/tc-12-1461-2018, 2018.

Henry-Edwards, A. and Tomczak, M.: Remote detection of water property changes from a time series of oceanographic data, Ocean Sci, 11–18 pp., 2006.

Ingram, R. G. and Larouche, P.: Variability of an under-ice river plume in Hudson Bay, J GEOPHYS RES-OCEANS, 92, 9541–9547, https://doi.org/10.1029/JC092iC09p09541, 1987.

Jones, E. P., Anderson, L. G., and Swift, J. H.: Distribution of Atlantic and Pacific waters in the upper Arctic Ocean: implications for circulation, Geophys Res Lett, 25, 765–768, https://doi.org/10.1029/98GL00464, 1998.

Mclaughlin, F., Carmack, E., Proshutinsky, A., Krishfield, R. A., Guay, C., Yamamoto-Kawai, M., Jackson, J. M., and Williams, B.: The Rapid Response of the Canada Basin to Climate Forcing: FROM BELLWETHER TO ALARM BELLS, Source: Oceanography, 24, 146–159, https://doi.org/10.2307/24861309, 2007.

Melling, H., Agnew, T. A., Falkner, K. K., Greenberg, D. A., Lee, C. M., Münchow, A., Petrie, B., Prinsenberg, S. J., Samelson, R. M., and Woodgate, R. A.: Fresh-Water Fluxes via Pacific and Arctic

Outflows Across the Canadian Polar Shelf, Climatic Change 115, 89–113. https://doi.org/10.1007/s10584-012-0576-4, 2012.

Newton, R., Schlosser, P., Mortlock, R., Swift, J., and MacDonald, R.: Canadian Basin freshwater sources and changes: Results from the 2005 Arctic Ocean Section, J Geophys Res Oceans, 118, 2133–2154, https://doi.org/10.1002/jgrc.20101, 2013.

Pardo, P. C., Pérez, F. F., Velo, A., and Gilcoto, M.: Water masses distribution in the Southern Ocean: Improvement of an extended OMP (eOMP) analysis, PROG OCEANOGR, 103, pp: 92-105, https://doi.org/10.1016/j.pocean.2012.06.002, September 2012.

Shimada, K., Itoh, M., Nishino, S., McLaughlin, F., Carmack, E., and Proshutinsky, A.: Halocline structure in the Canada Basin of the Arctic Ocean, Geophys Res Lett, 32, 1–5, https://doi.org/10.1029/2004GL021358, 2005.

Stigebrandt, A. The North Pacific_ A Global-Scale Estuary, J PHYS OCEANOGR, 14(2), 464-470. https://journals.ametsoc.org/view/journals/phoc/14/2/1520-0485_1984_014_0464_tnpags_2_0_co_2.xml, 1984.

Tomczak, M. and Liefrink, S.: Interannual variations of water mass volumes in the Southern Ocean, Journal of Atmospheric and Ocean Science, 10, 31–42, https://doi.org/10.1080/17417530500062838, 2005.

Whitmore, L. M., Pasqualini, A., Newton, R., and Shiller, A. M.: Gallium: A New Tracer of Pacific Water in the Arctic Ocean, J Geophys Res Oceans, 125, https://doi.org/10.1029/2019JC015842, 2020.

Zhang, J., Weijer, W., Steele, M., Cheng, W., Verma, T., and Veneziani, M.: Labrador Sea freshening linked to Beaufort Gyre freshwater release, Nat Commun, 12, https://doi.org/10.1038/s41467-021-21470-3, 2021.

Zhuang, Y., Jin, H., Cai, W. J., Li, H., Jin, M., Qi, D., and Chen, J.: Freshening leads to a three-decade trend of declining nutrients in the western Arctic Ocean, ENVIRON RES LETT, 16, https://doi.org/10.1088/1748-9326/abf58b, 2021.